

Conserved Residues in the Extracellular Loops of Short-Wavelength Cone Visual Pigments

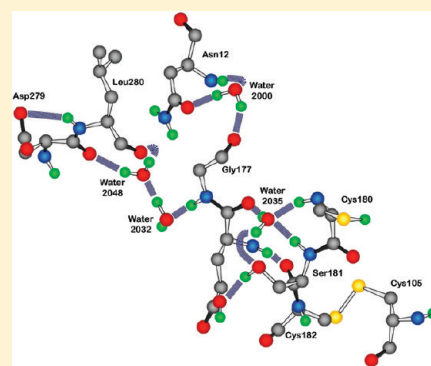
Min-Hsuan Chen,[†] Daniel J. Sandberg,[§] Kunnel R. Babu,[†] Jose Bubis,[‡] Arjun Surya,[†] Lavoisier S. Ramos,[§] Heidi J. Zapata,[†] Jhenny F. Galan,[§] Megan N. Sandberg,[§] Robert R. Birge,^{*,§} and Barry E. Knox^{*,†}

[†]Department of Biochemistry and Molecular Biology and Department of Ophthalmology, SUNY Upstate Medical University, Syracuse, New York 13210, United States

[‡]Departamento de Biología Celular, Universidad Simón Bolívar, Caracas, Venezuela

[§]Department of Chemistry and Department of Molecular and Cell Biology, University of Connecticut, Storrs, Connecticut 06269, United States

ABSTRACT: The role of the extracellular loop region of a short-wavelength sensitive pigment, *Xenopus* violet cone opsin, is investigated via computational modeling, mutagenesis, and spectroscopy. The computational models predict a complex H-bonding network that stabilizes and connects the EC2–EC3 loop and the N-terminus. Mutations that are predicted to disrupt the H-bonding network are shown to produce visual pigments that do not stably bind chromophore and exhibit properties of a misfolded protein. The potential role of a disulfide bond between two conserved Cys residues, Cys¹⁰⁵ in TM3 and Cys¹⁸² in EC2, is necessary for proper folding and trafficking in VCOP. Lastly, certain residues in the EC2 loop are predicted to stabilize the formation of two antiparallel β -strands joined by a hairpin turn, which interact with the chromophore via H-bonding or van der Waals interactions. Mutations of conserved residues result in a decrease in the level of chromophore binding. These results demonstrate that the extracellular loops are crucial for the formation of this cone visual pigment. Moreover, there are significant differences in the structure and function of this region in VCOP compared to that in rhodopsin.



The visual pigments make up a class of guanine protein-coupled receptors (GPCRs) that initiate phototransduction in retinal photoreceptors. Each protein consists of seven transmembrane α -helices connected by surface-exposed loops and an 11-*cis*-retinal chromophore.^{1–4} Following absorption of light, the retinal chromophore, covalently bound to a conserved lysine residue in transmembrane helix 7 (TM7), isomerizes from the 11-*cis* to the all-*trans* conformation to trigger a series of conformational changes in the tertiary structure of the protein that lead to the formation of the active state, R* or meta II. The corresponding conformational changes in the covalently bound opsin polypeptide initiate a secondary messenger cascade within the photoreceptor that results in the changes in plasma membrane potential and synaptic transmission.^{5–10}

Both rod and cone visual pigments contain conserved residues located in the extracellular loop regions that interact with proteins involved in phototransduction. The cytoplasmic domain (CP), formed by four loops tethered to the lipid bilayer with a flexible carboxyl terminus, contains several palmitoylated Cys residues as well as multiple Ser and Thr residues that serve as targets for GRK phosphorylation.¹¹ In the case of bovine rhodopsin, a significant portion of the CP domain is involved in the light-dependent interactions with transducin,^{12–14} GRK1,¹⁵ and arrestin.¹⁶ The high degree of homology in the CP loop regions of the cone opsins with rhodopsin indicates that cone opsins will exhibit many of the same structure–function relationships as rhodopsin.

Recent studies have indicated that the extracellular (EC) loop regions of GPCRs have an equally important role in proper protein folding and trafficking.^{1,4,17} Mutations in the EC2 loop of bovine rhodopsin, which penetrates the chromophore binding crevice and stabilizes the overall helical bundle, have either (1) induced a shift in the wavelength of the absorption maximum, (2) destabilized retinal binding, (3) caused a defect in N-linked glycosylation and protein trafficking, or (4) caused retinitis pigmentosa.^{18–25} In the medium- and long-wavelength sensitive (M/LWS) cone opsins, an anion binding site is formed partly by the EC2 loop and regulates spectral and photobleaching properties.²⁶ NMR analysis indicates the EC2 loop of rhodopsin forms a cap over the chromophore, which exhibits structural changes upon light activation. Furthermore, the β 4 strand in EC2 interacts with TM4–TM6 during photoactivation.²⁷ The EC loops not only stabilize the protein and facilitate the proper photobleaching but also function to stabilize ligand binding in other receptors.^{28,29}

Elucidation of EC loop function remains a primary objective toward a complete mechanistic understanding of GPCR activation. Although the crystal structure of bovine rhodopsin is known with high resolution, the flexibility in the EC loops suggests the

Received: September 24, 2010

Revised: June 19, 2011

Published: June 20, 2011

crystal structure is just a snapshot of one of several possible conformations. Monte Carlo simulated temperature annealing combined with a scaled collective variable technique has been employed to search the conformation space for loop structures,³⁰ revealing the crystal structure could be one conformation in the native ensemble. Geometric sampling and energy minimization have also been used to specifically study the loop regions in both the R and R* states of rhodopsin.^{31–33} Collectively, these studies exemplify the means by which theoretical computation can be combined with emerging experimental data to study the function of EC residues.

Although a major effort has been made toward the study of rhodopsin EC loop residues, cone opsins warrant equally intense investigation because of their important role in daylight vision, significant differences in the spectral, photoactivation, and chromophore binding compared to that with rhodopsin, and potential clinical problems associated with human mutations. *Xenopus* violet cone opsin (VCOP) has been an important model cone opsin for biochemical and biophysical studies, for a number of reasons. The complete photobleaching pathway of the pigment and protonation state of the Schiff base in the dark state have been determined.^{34,35} Additionally, the pigment has shown an ability to activate transduction, and the apoprotein is able to regenerate 11-*cis*-retinal more efficiently than other cone opsins.³⁶ Furthermore, the retinylidene Schiff base counterion has been identified, and the role of this residue in regulating the photobleaching cascade has been investigated. Using a combination of mutagenesis, spectroscopy, molecular dynamics simulations, semiempirical modeling, and homology modeling, this treatment elucidates the role of the EC2 and EC3 loops in cone opsins and provides insight into the role of the EC loop regions in protein folding.

MATERIALS AND METHODS

Homology Modeling of VCOP. The crystal structure of bovine rhodopsin (chain A from Protein Data Bank entry 1U19)¹ was used as the template for modeling the three-dimensional structure of VCOP. The sequence alignment of rhodopsin, VCOP, and VCOP homology models was generated using Modeler.³⁷ Hydrogen atoms, a protonated Schiff base linkage between Lys²⁹¹ and 11-*cis*-retinal, and a disulfide linkage between Cys¹⁰⁵ and Cys¹⁸² were added using the visualization program VMD.³⁸ Thirty-six internal hydration water molecules were introduced using both a comparison between the rhodopsin crystal structure and those predicted by DOWSER.³⁹ DOWSER detected 20 internal hydration sites for VCOP, five of which closely match with the crystal structure water molecules (2000, 2020, 2021, 2024, and 2028). The complete VCOP homology model with internal hydration water molecules was minimized for 4000 steps using NAMD.⁴⁰ A lipid bilayer was included in the model to simulate the unsaturated phospholipids of the outer segment of the rod photoreceptor.⁴¹ The protein was embedded in a POPC (palmitoylcholine) lipid box (90 Å × 90 Å) using VMD. Lipid molecules overlapping with the protein were removed, and the final model contained 169 POPC molecules. A short molecular dynamics (120 ps) was performed on the protein–membrane system to relax the protein–lipid interface. The entire system was then solvated with water molecules (TIP3) using VMD. The fully solvated system was 90 Å × 90 Å × 100 Å in size and contains 13542 water molecules. To neutralize the system, 38 sodium and chloride ions were

added and manually redistributed on the basis of the surface potential map generated by GRASP.⁴²

Molecular Dynamics Simulations. All molecular dynamics simulations were conducted with full particle-mesh Ewald (PME) calculation for electrostatic interactions. To fully relax the system, the simulations were conducted systematically as follows: 25 ps with the protein fixed, 25 ps with the entire protein harmonically constrained, 25 ps with the peptide backbone harmonically constrained, 25 ps with α -carbons harmonically constrained, and finally 25 ps with only retinal constrained. An NPT ensemble (constant pressure and temperature) simulation was then performed for 2 ns. The calculations were conducted using an SGI Altix 350 server (12 Intel Itanium 2 CPUs), and the time required for the 1 ns simulation was 36 h. Thermal noise reduction was performed by sliding a window of nine frames on the trajectory file using a modified VMD script developed but unpublished by J. Saam.⁴³ To compare different models, structural alignment of proteins was performed using the STAMP algorithms⁴⁴ built within VMD (solvent water molecules, POPC molecules, and ions removed prior to comparison). Hydrogen bonds (<2.5 Å) were identified using “HBOND” in DS ViewerPro. All minimizations and molecular dynamics simulations were performed using NAMD. The CHARMM27 force field was used for proteins and lipids and TIP3P for water molecules. All titratable groups were assigned protonation states according to the CHARMM force field.³⁸ Asp¹⁰⁸ was assumed to be unprotonated.⁴⁵

Semiempirical Approximation of the Enthalpy of Formation. The enthalpy of formation for each mutant and that for the wild-type (WT) VCOP protein were estimated by using routines from the MOPAC software package.⁴⁶ The model built for the aforementioned CHARMM molecular dynamics simulations was employed as a starting structure for all calculations. Mutations to the WT model were made via tools included in Swiss PDB,⁴⁷ and a steepest decent minimization algorithm was employed for geometry optimization. The PM6 Hamiltonian⁴⁸ energy was evaluated via standard self-consistent field minimization methods, and the enthalpy of formation was calculated as described in ref 46. Structural analysis of the energy-minimized protein geometry was accomplished via programs coded in extended basic, using the MathScriptor compiler (R. R. Birge, unpublished and available upon request). Computations were performed on a Microway Opteron computer cluster with ten 32 GB AMD Quad Opteron 2350 processors running Fedora Core 8. Each minimization required 3–6 days of computation time.

Sequence Comparisons. The consensus sequences for the regions including the EC2 loop (amino acids 177–199 of bovine rhodopsin), the C-segment of TM6, the EC3 loop, and the N-segment of TM7 (amino acids 266–296 of bovine rhodopsin) were obtained for each of the five vertebrate opsin families from the G-protein-coupled receptor database.⁴⁹ Alignments were prepared using Clustal X methods as implemented in MegAlign (DNAStar).

Preparation and Expression of VCOP Mutants. The 1D4 epitope-tagged VCOP plasmids used for mutagenesis and expression have been described previously.⁴⁵ The 1D4 epitope is not present in WT VCOP but has been added in place of the WT carboxyl terminus. All amino acid changes were made by restriction fragment replacement: single and double D279Q and L280P using NcoI and SacI, R281Q using BglII and SacI, and Y269F and the chimeric constructs using EaeI and NcoI. The sequences of the resulting mutant plasmids were verified. The resulting plasmids

had the cDNA containing the codons encoding the first 328 amino acids of the mutant VCOP fused in frame with the codons encoding the last 14 amino acids of bovine rhodopsin, which serves as an epitope tag.⁵⁰ The mutants were expressed in COS1 cells by transient transfection, purified by immunoaffinity chromatography, and analyzed as previously described.^{34,36} Pigments were eluted in buffer Y1 [50 mM HEPES, 140 mM NaCl, and 3 mM MgCl₂ (pH 6.6)] with 0.1% DM and 20% glycerol.

UV-Vis Spectroscopy. Conventional UV-vis spectroscopy was conducted using a Beckman DU-640 spectrometer at 22 °C.³⁶ We determined light-dark difference spectra by collecting four spectra in the dark, bleaching the samples with white light from a projector lamp (300 W, EXR-5, Wiko, Inc.) for 1 min, and subsequently recording four spectra. The total radiant energy of the white light was measured to be 8 mW using an optometer (Graseby Optronics). Subtraction of light scattering using a λ^{-4} correction factor was done for all spectra using FitSpectra (R. R. Birge, unpublished and available upon request). Light-dark difference spectra were calculated using four averaged spectra using SigmaPlot (Jandel Scientific).

Western Blots and Immunohistochemistry. Purified protein samples were diluted into buffer containing 4% SDS, resolved on 10% polyacrylamide gels, transferred to nylon membranes, and detected with the anti-rhodopsin monoclonal antibody, 1D4. Samples were kept below room temperature prior to solubilization with SDS and electrophoresis. Bound antibody was detected by chemiluminescence (Amersham ECL kit).

RESULTS AND DISCUSSION

Alignment of the EC2 loop consensus sequences for each of the subfamilies of visual pigments (Figure 1), compared to the EC2 loop consensus sequence of rhodopsin-like type 1 pigments (Rh1), indicated rhodopsin-like type 2 pigments (Rh2) were 83% homologous, short-wavelength sensitive type 1 pigments (SWS1) ~60%, short-wavelength sensitive type 2 pigments (SWS2) ~65%, and medium- to long-wavelength sensitive pigments (M/LWS) ~39%. Seven conserved residues within the EC2 loop among all the opsin families are noted: Arg¹⁷⁷, Pro¹⁸⁰, Gly¹⁸², Ser¹⁸⁶, Cys¹⁸⁷, Gly¹⁸⁸, and Asp¹⁹⁰ (using the sequence numbers of rhodopsin, the protein for which the structural roles of these conserved residues have been previously reported).^{2,4,51} As opposed to the EC2 loop, the EC3 loop shares no conserved residues and displays little primary sequence identity between the different opsin families. The EC3 loop in our VCOP model spans only seven residues, extending out of TM6 at Arg²⁷⁴, pivoting at Gly²⁷⁷, and returning to TM7 at Leu²⁸⁰.

Experimental Analysis of *Xenopus* Violet Cone Opsin Mutants. To evaluate the potential role of particular amino acid residues in the structure and function of VCOP, we characterized protein expressed in a well-established heterologous system based upon transfection of COS1 cells (see Materials and Methods). Mutant proteins purified from transfected COS1 cells were analyzed by denaturing polyacrylamide electrophoresis to determine the post-translational glycosylation status. Bovine rhodopsin and VCOP cells exhibit a strong immunoreactive band with an apparent molecular mass of ~34–35 kDa and an associated broad smear of immunoreactive protein up to ~45 kDa (Figure 2). For both rhodopsin and VCOP, these bands are heterogeneously glycosylated with a mixture of complex carbohydrates that can be partially removed by digestion with PNGaseF.^{36,39,52} In addition, VCOP produces more dimer

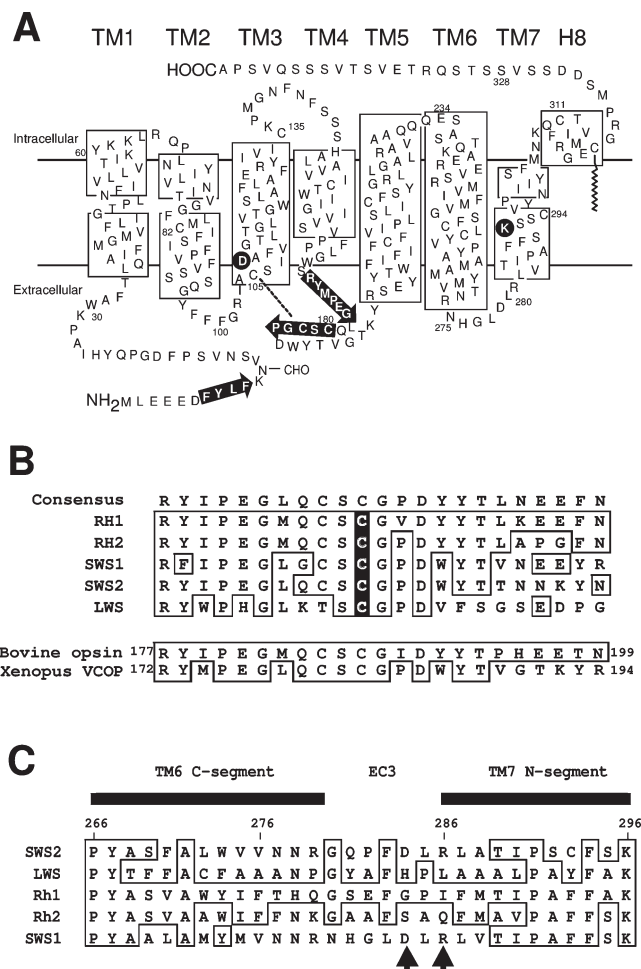


Figure 1. (A) Secondary structural model of *Xenopus* violet cone opsin (VCOP). Predicted α -helical regions, based upon homology modeling, are boxed, and the seven transmembrane helices (TM) are labeled. Black arrows denote predicted β -strands. The conserved lysine residue (K²⁹¹) in TM7 to which 11-*cis*-retinal is covalently bound and the aspartic acid residue (D¹⁰⁸) that serves as the counterion to the protonated Schiff base are highlighted with black circles. Post-translation modification of N¹⁵ (glycosylation) is indicated by CHO and palmitoylation of C³¹⁷ by a jagged line. (B) Comparison of the consensus EC2 loop sequences for the five vertebrate visual pigment families. The composite consensus sequences were generated using a majority rule. The composite consensus sequence for the visual pigments is listed first (Consensus), followed by rhodopsin-like type 1 (RH1), rhodopsin-like type 2 (RH2), short-wavelength sensitive set 1 (SWS1), short-wavelength sensitive set 2 (SWS2), and long- or medium-wavelength sensitive (LWS). The bovine opsin and VCOP EC2 loop sequences are shown for comparison. Residues conserved in a majority of cases are boxed. A highly conserved cysteine residue (C¹⁸⁷ in bovine rhodopsin) is highlighted in black. (C) Consensus sequences of the EC3 loop of visual pigments. The consensus sequences for each family of visual pigment were generated by majority rule. There were no amino acids conserved in all five visual pigments. D²⁷⁹ and R²⁸¹ from VCOP are denoted with arrows.

(~75 kDa) than rhodopsin in these SDS gels. The mutants studied here exhibited a range of patterns in the electrophoretic analysis. Representative mutants are shown in Figure 2. Some mutants (e.g., E176D and S181A) had patterns similar to that of WT VCOP, while others (C105A, C182A, D279Q, and R281Q) showed an absence of the broad smear. Mutants in the latter class apparently have a deficiency in post-translational glycosylation

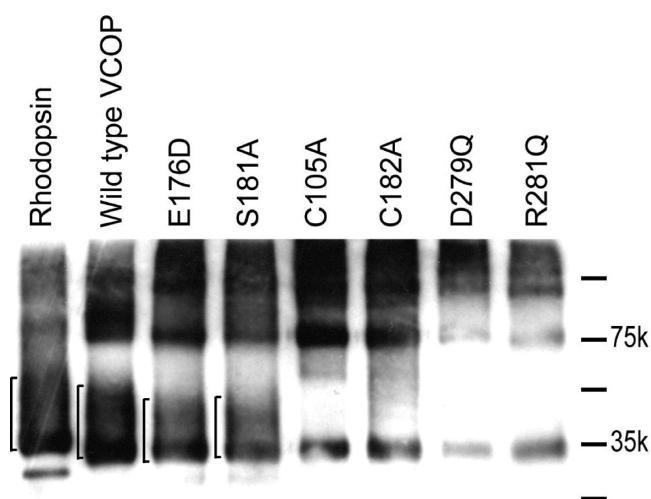


Figure 2. Western blot of visual pigments heterologously expressed in COS1 cells. Equal amounts of purified visual pigments were resolved via sodium dodecyl sulfate–polyacrylamide gel electrophoresis and detected using a monoclonal antibody that recognizes the C-terminus of all constructs. Bovine rhodopsin (Rhodopsin) and normal (Wild type) VCOP migrate with multiple species, including a monomer at ~ 34 kDa and a smear of heterogeneously glycosylated monomers highlighted with a bracket. VCOP also exhibits a significant dimer that runs at ~ 85 kDa. VCOP single-amino acid substitution mutants have a diversity of patterns. Mutants E176D and S181A have the same pattern as WT VCOP, while mutants C105A, C182A, D279Q, and R281Q all exhibit a significant reduction in the broadly glycosylated protein between the monomeric and dimeric species. The molecular mass standards were 25, 35, 50, 75, and 100 kDa.

that is possibly caused by a protein processing defect associated with protein misfolding in the endoplasmic reticulum or Golgi. These results show that a number of EC2 and EC3 mutants play a significant role in the biosynthesis of VCOP.

All VCOP mutants were purified by immunoaffinity chromatography in dodecyl maltoside following addition of 11-*cis*-retinal to cells, and the resulting protein was analyzed by UV–visible spectroscopy. We observed three different mutant phenotypes (Table 1) as judged by chromophore binding: indistinguishable from WT VCOP, reduced chromophore, and no detectable chromophore bound. Those mutants with chromophore bound to some level are shown (Figure 3), and their spectral properties are summarized in Table 1. In addition to the amount of bound chromophore, several of the mutants showed a slightly altered λ_{\max} compared to the value for WT VCOP, ~ 427 nm. Cone pigments differ from rhodopsins in their reactivity to hydroxylamine in the dark, and this is thought to reflect different accessibilities of the solvent to the Schiff base local environment. Rhodopsins are essentially nonreactive in the dark, while cone opsins rapidly lose their chromophore in the dark. We measured the rate of chromophore hydrolysis in the presence of hydroxylamine for the EC3 mutants that generated a good yield of pigment. Under conditions of excess hydroxylamine and at room temperature, for all of the mutants tested the half-times of chromophore decay were between 5 and 9 min; WT VCOP had a half-time of 7.5 min (data not shown). Additional discussion of the mutant spectroscopic results is given below.

Computationally Predicted Hydrogen Bond Networks. To aid in our understanding the role of EC2 and EC3 residues in the structure and function of VCOP in the absence of a high-

resolution structure, we utilized computational modeling (see Materials and Methods). The equilibrated VCOP model is stable and offers a suitable means for inferring the function of key residues. The relaxation of the model helical bundle showed an expansion of the system volume by 262 \AA^3 , compared to that of the rhodopsin crystal structure, to a total volume of 33972 \AA^3 . Very little movement in the residues forming the binding pocket was observed during molecular dynamics (MD) equilibration, and the retinal, despite exhibiting minor stretching and bending of the polyene chain during the MD, showed no loss of planarity or isomerization. The Asp¹⁰⁸ residue, the primary counterion to the protonated Schiff base, interacts with the charged moiety within a distance of 1.8 \AA . Furthermore, 13 of the 36 crystal water molecules remained in position, all of which bridge amino acids. The backbone trace for the N-terminus of the model deviated by only 3.8 \AA from the rhodopsin crystal structure, though a significant difference in the orientation of the amino acids was observed. The VCOP EC2 loop is predicted to contain two antiparallel β -strands, labeled $\beta 3$ (Arg¹⁷²–Glu¹⁷⁶) and $\beta 4$ (Ser¹⁸¹–Asp¹⁸⁵), connected by a hairpin linker, ¹⁷⁷GLQC¹⁸⁰, facilitated by Gly¹⁷⁷ identical in size and structure to rhodopsin's ¹⁷⁷GMQC¹⁸⁰ linker (Figure 4). However, the $\beta 4$ strand of VCOP shows no intramolecular interaction with the chromophore, as in rhodopsin. Thus, the computational modeling predicts a structural element that is significantly different from that of bovine rhodopsin, namely the absence of contacts between EC2 and 11-*cis*-retinal. This may have an important consequence for the stability of retinal in the binding pocket and highlights a key difference between rod and cone pigments.

The VCOP model predicts the EC2 loop has hydrogen bonds to the EC3 loop, via Asp²⁷⁹ and Leu²⁸⁰, which itself is bonded to Asn¹² in the N-terminus. In rhodopsin, the EC3 loop is also predicted to form a H-bond network with the N-terminus but not with the EC2 loop. The VCOP network involves Asn¹², Gly¹⁷⁷, Asp²⁷⁹, Leu²⁸⁰, and three water molecules. This H-bonding pattern orients the EC2 and EC3 loops over the retinal, introducing an H-bond between Ser¹⁸¹ and Asp¹⁰⁸, dictating the protein–chromophore interaction. The VCOP model predicts that, contrary to the X-ray crystal structure of bovine rhodopsin, the EC2 loop is indirectly H-bonded to the N-terminus via EC3 loop amino acids Asp²⁷⁹ and Leu²⁸⁰, highlighting a novel function for the short EC3 loop. Arg²⁸¹ does not interact with any residue but is exposed to the solvent that determines the proper axial orientation for TM7 in the membrane. The importance of these residues in protein folding and stabilizing the binding of 11-*cis*-retinal was evident in replacements involving either Asp²⁷⁹ or Arg²⁸¹ individually or in combination. PM6 energy minimization predicted neutralizing either residue in the charged pair individually was enthalpically unfavored, whereas the double mutation was slightly favored (see Table 1). Exchanging the positions of the two charged residues in the double mutant D279R/R281D yielded a misfolded protein as well, indicating residues Asp²⁷⁹ and Arg²⁸¹ are not simply involved in forming a single intramolecular salt bridge. These results demonstrate the necessity for this conserved charged pair for proper protein folding in VCOP and support the extended hydrogen bonding network predicted by the computational modeling. Leu²⁸⁰ is predicted to be another vital residue in the EC3-DLR motif. The experimental results for L280P, L280G, and L280A support this function. The L280P and L280G models (Figure 4) suggest that the mutant at position 280 causes Thr²⁸⁴ in TM7 to directly interact with EC2 loop residues Leu¹⁷⁸ and Glu¹⁷⁶. The L280P

Table 1

| | $\Delta\lambda_{\max}$ (nm) ^a | $A(\lambda_{\max})/A(\lambda_{280})$ ^b | $\Delta(\Delta\text{HOF})$ (kcal/mol) ^c | shift of key residues (Å) ^d | $\Delta\beta 3$ length (Å) ^e | $\Delta\beta 4$ length (Å) ^e | $\Delta\text{hairpin turn}$ (deg) ^f |
|------------------|--|---|---|---|--|--|---|
| wild type | $\lambda_{\max} = 427$ nm | 1, normalized | $\Delta H = -23264$ | 0 | 0 | 0 | 0 |
| C105A | N/A ^g | 0 | -77 | 0.781 | 0.325 | -0.067 | -0.394 |
| C180A | -9.5 | 0.490 | -4 | 0.247 | 0.000 | -0.002 | 0.002 |
| C182A | N/A ^g | 0 | 180 | 0.637 | 0.392 | -0.064 | -0.495 |
| C180A/C182A | -18 | 0.141 | 238 | 0.507 | 0.001 | -0.009 | -0.007 |
| L178A | -7 | 0.397 | 322 | 0.956 | 0.348 | -0.058 | -0.705 |
| L178D | N/A ^g | 0 | 152 | 0.523 | -0.755 | 0.295 | 0.512 |
| L178H | -16.5 | 0.178 | 619 | 0.620 | 0.433 | -0.043 | 0.812 |
| L178M | -0.5 | 0.686 | 468 | 0.349 | 0.938 | -0.058 | 0.295 |
| P184I | -2 | 0.485 | 262 | 0.846 | 0.140 | -0.172 | 12.847 |
| W186Y | N/A ^g | 0 | 402 | 0.411 | 0.571 | -0.079 | -0.821 |
| E176D | -13.5 | 0.104 | 395 | 0.686 | 0.370 | -0.295 | -0.935 |
| E176H | N/A ^g | 0 | 685 | 0.868 | 0.521 | -0.044 | -1.602 |
| E176G | N/A ^g | 0 | 333 | 1.020 | 0.463 | -0.022 | -1.046 |
| E176Q | N/A ^g | 0 | 332 | 0.942 | 0.325 | 0.017 | -1.270 |
| E176S | N/A ^g | 0 | 322 | 0.956 | 0.348 | -0.058 | -0.706 |
| E176D/S181T | N/A ^g | 0 | -17 | 0.466 | 0.005 | 0.004 | 0.078 |
| E176S/S181E | N/A ^g | 0 | 158 | 1.140 | -0.668 | -0.219 | 2.136 |
| E176G/L178E | -18 | 0.114 | 198 | 0.521 | -0.001 | -0.003 | 2.080 |
| S181A | N/A ^g | 0 | 443 | 0.604 | 0.525 | 0.117 | -0.961 |
| S181C | N/A ^g | 0 | 50 | 0.078 | 0.001 | 0.000 | 0.003 |
| S181E | N/A ^g | 0 | -101 | 0.040 | -0.002 | 0.002 | 0.017 |
| S181T | N/A ^g | 0 | 280 | 0.546 | 0.476 | -0.063 | -0.958 |
| D279Q | N/A ^g | 0 | 757 | 0.576 | 0.448 | -0.228 | -0.955 |
| R281Q | N/A ^g | 0 | 176 | 0.775 | 0.455 | -0.222 | -1.042 |
| D279Q/R281Q | N/A ^g | 0 | -82 | 0.376 | 0.000 | 0.000 | 0.000 |
| D279R/R281D | N/A ^g | 0 | 173 | 0.518 | 0.000 | 0.000 | 0.000 |
| L280A | 1 | 0.250 | 438 | 0.561 | 0.490 | -0.162 | -0.889 |
| L280G | -1 | 0.150 | 414 | 0.773 | 0.442 | -0.206 | -0.890 |
| L280P | -17 | 0.980 | 419 | 0.727 | 0.467 | -0.200 | -0.846 |
| BOP-VCOP chimera | N/A ^g | 0 | -1446 | 3.843 | -0.478 | -2.431 | 4.199 |
| chimera W186Y | N/A ^g | 0 | -1420 | 4.101 | -0.525 | -2.513 | 3.885 |

^a A negative $\Delta\lambda_{\max}$ indicates a blue shift. ^b For each mutant, the absorbance at the mutant's λ_{\max} was divided by the absorbance of the amino acids at λ_{280} . The ratio $A(\lambda_{\max})/A(\lambda_{280})$ for each mutant was then divided by the same ratio for the WT protein to normalize WT to unity. ^c The enthalpy of formation of the WT protein was subtracted from the enthalpy of formation of the mutant protein. Therefore, a negative $\Delta(\Delta\text{HOF})$ indicates the mutant protein is more enthalpically favored than the WT protein. ^d The shift in the center of mass of charged residues and residues within 5 Å of the chromophore was determined. The chromophore was used to align the WT and mutant proteins. ^e The length of each β -strand was determined by calculating the distance between the center of mass of the residues at either end of each strand. ^f The angle between β -strands was calculated by creating vectors for each β -strand, determined by the center of mass of the residues belonging to the strand. The two vectors were then used to trigonometrically determine the angle between them. ^g Not available.

model predicts a disruption in the H-bonding interaction between the N-terminus and the EC loops. As shown in Figure 5, Pro²⁸⁰ is predicted to have a main chain–side chain interaction with Thr²⁸⁴, extended to main chain–main chain interactions with Arg²⁸¹ in the EC3 loop as well as side chain–side chain interactions with Glu¹⁷⁶, none of which were present in the WT VCOP model (Figure 4). The aberrant H-bonding network in L280P causes a water molecule previously H-bonded to Asp¹⁰⁸ to H-bond to Ser¹⁸¹, potentially destabilizing the primary counterion of the retinal. Furthermore, Pro²⁸⁰ interacts primarily with the transmembrane domain, whereas Leu²⁸⁰ interacts with the extracellular domain. A root-mean-square deviation (rmsd) analysis of the position of the atoms in the EC3 loop, throughout the 2 ns MD simulation, yielded an ~ 2 Å shorter movement for the L280P mutant

compared to WT, indicating the mutant contains more rigidity in the EC3 loop. Calculations indicate the mutation is enthalpically unfavored.

The L280G model contains a H-bonding network similar to the L280P mutant H-bonding network. As in L280P, the introduction of Gly at position 280 provides enough flexibility for the EC3 loop to interact more strongly with the helical bundle and more weakly with the N-terminus compared to WT. The L280G mutant has a main chain–side chain interaction with Thr²⁸⁴, in TM7, and a main chain–main chain interaction with Asp²⁷⁹ (Figure 5). The water molecules bridging H-bonds from Glu¹⁷⁶, as observed in both L280P and WT models, have dissociated from the protein and into the bulk simulation box. This mutation was computed to be enthalpically unfavored.

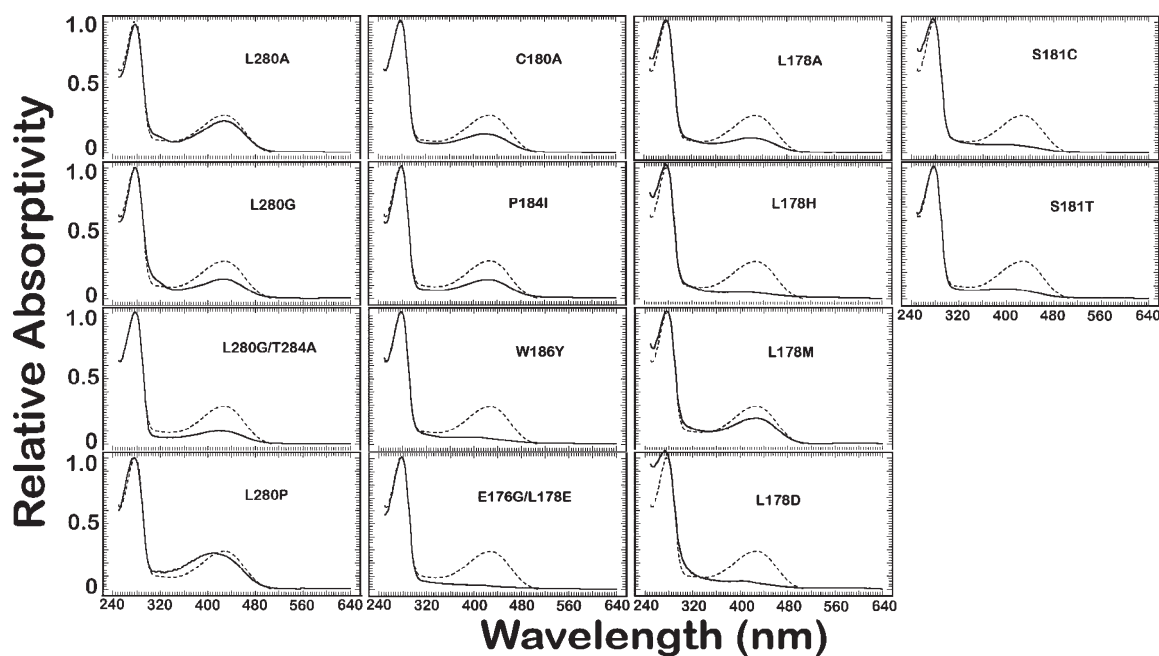


Figure 3. UV-vis spectroscopy of single-amino acid substitution mutants in EC2 and EC3 loops. Following addition of 11-*cis*-retinal, mutant proteins were purified in dodecyl maltoside, and UV-vis spectra were recorded (black lines). For comparison, a spectrum of WT VCOP is presented in each panel (gray lines). Absorption at 280 nm arises from aromatic amino acids of protein, while absorption above ~ 300 nm arises from the bound chromophore. The inset shows the chromophore region of the spectrum expanded to show the pigment bound at reduced levels compared to that of the wild type. Each spectrum was normalized to have a relative OD of 1.0 at 280 nm to facilitate comparisons between different protein samples. There was a wide range of pigment formation, from nearly wild-type levels (e.g., L280A) to barely detectable (e.g., W186Y). The fraction of protein that binds the chromophore can be quantified by the ratio of the absorbance at 425 nm to that of the protein at 280 nm (see Table 1).

Further computations and experiments supported the importance of the EC3 loop. A double mutant, L280G/T284A, failed to improve the level of retinal binding and induced an ~ 13 nm red shift in λ_{\max} compared to that of WT. The double mutant model predicts a major disturbance in the interactions between the EC2 and EC3 loops (Figure 5), leading to a random coil-like structure instead of the β -strands in the EC2 loop (Figure 5) and neutralization of the side chains of Asp²⁷⁹ and Arg²⁸¹ (Figure 5). In summary, direct changes to the H-bonding network residues in the EC loops increase the flexibility of the region and possibly destabilize the chromophore binding crevice, thus weakening interactions with the 11-*cis*-retinal. The computational models highlight the vital function of residues Asp²⁷⁹, Leu²⁸⁰, and Arg²⁸¹ and suggest the reason mutations to these residues weaken chromophore binding.

Disulfide Linkage between Cys¹⁰⁵ and Cys¹⁸². The VCOP model was constructed with a disulfide bond between Cys¹⁰⁵ and Cys¹⁸², highly conserved residues in all visual pigments. Mutations of these two residues produced misfolded protein rather than specific destabilized retinal binding. Supporting evidence for this disulfide bond was obtained from UV-vis spectra: C105A and C182A mutants had no detectable chromophore in purified samples, while the C180A mutant bound chromophore, albeit at a reduced level compared to that of the wild type, with a 10 nm blue-shifted λ_{\max} (Figure 3). Computationally, the C105A mutation was predicted to be enthalpically favored, the C180A mutation was enthalpically null, and the C182A mutation was enthalpically disfavored. The double mutant C180A/C182A, also predicted to be enthalpically disfavored, did not bind the chromophore. These experiments strongly suggest that, in the WT VCOP protein, Cys¹⁰⁵ and Cys¹⁸² are covalently

interconnected via a disulfide linkage. These results further suggest that the disulfide bond is essential for proper folding and post-translational processing in the endoplasmic reticulum. In bovine rhodopsin, comparable Cys to Ala mutants fold and bind the chromophore but with the reduced stability of meta II.²³ The formation of an abnormal disulfide bond between Cys¹⁸⁵ and Cys¹⁸⁷ has been identified in a misfolded rhodopsin.⁵³

The VCOP model predicts a H-bonding network within EC2 (Figure 6) that includes residues Cys¹⁰⁵, Cys¹⁸⁰, Ser¹⁸¹, and Cys¹⁸² and the backbone oxygen of Gly¹⁷⁷ H-bonded to the H of water 2035. The H-bonding network within EC2 is then directed over the chromophore by Cys¹⁸² that is presumably assigned a disulfide linkage to Cys¹⁰⁵ in TM3. The computational models correctly predict the cysteine residues form a disulfide linkage. Experimental data about the stability of VCOP mutant proteins support these predictions.

Binding Site Residues Glu¹⁷⁶ and Ser¹⁸¹. Two residues, Glu¹⁷⁶ and Ser¹⁸¹, are strongly conserved in visual pigments. In contrast to Glu¹⁸¹ in bovine rhodopsin, the VCOP model suggests that the equivalent residue, Glu¹⁷⁶, does not have any direct intramolecular interaction with the polyene chain of 11-*cis*-retinal. However, Glu¹⁷⁶ is predicted to H-bond to Ser¹⁸¹ strongly to stabilize the $\beta 3$ - $\beta 4$ hairpin, to Tyr²⁶³, and through side chains to align the $\beta 4$ strand in the binding crevice (Figures 5 and 6). All four mutations of Glu¹⁷⁶ (to D, Q, H, and S) prevented stable chromophore binding. All single mutations of Glu¹⁷⁶ are predicted to be enthalpically disfavored despite little change in the overall structure of the protein. Mutation of Ser¹⁸¹ also had severe effects, although S181T and S181C did bind retinal at a very reduced level. Double mutants (E176D/S181T and E176S/S181E) could not compensate for the deficiency in retinal binding in either single

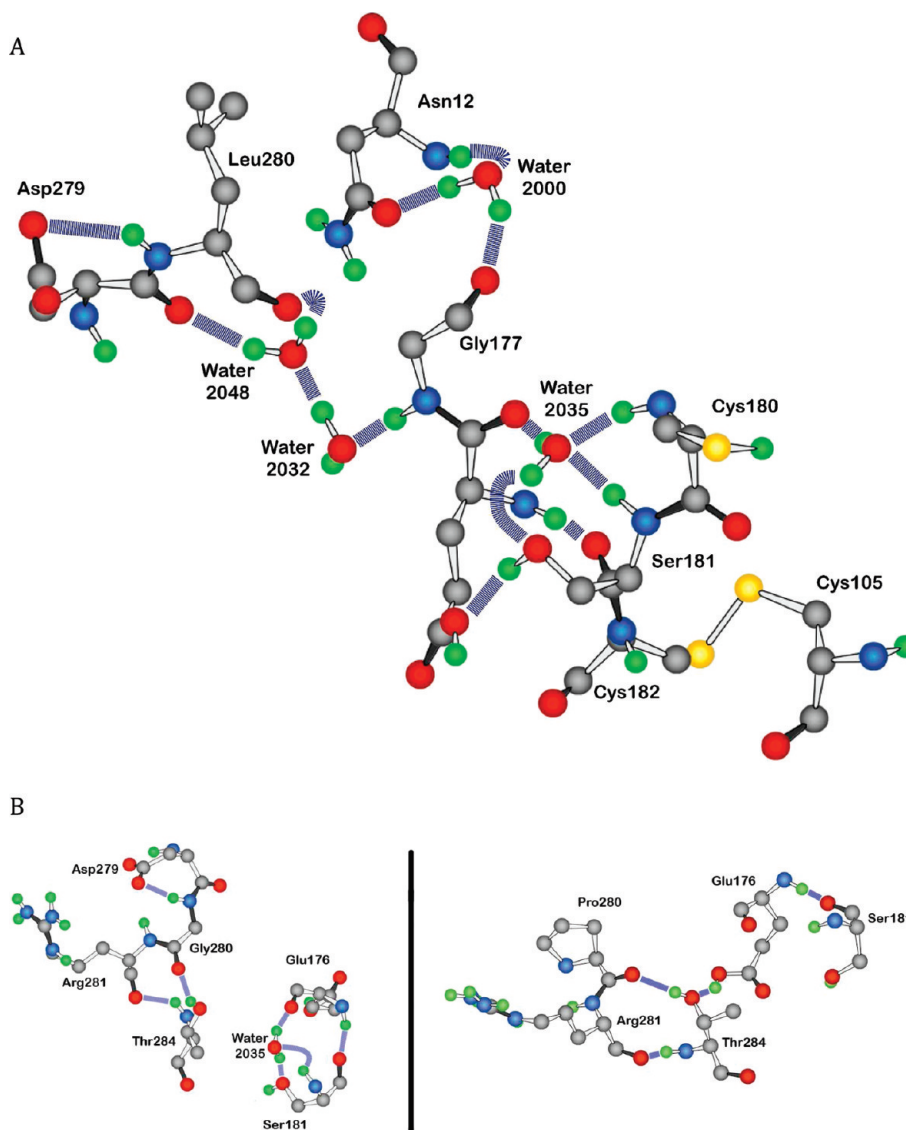


Figure 4. (A) Predicted hydrogen bonding network derived from homology modeling in the extracellular domain of VCOP. Critical residues (Asn¹², Gly¹⁷⁷, Asp²⁷⁹, and Leu²⁸⁰) were distributed among EC2, EC3, and the N-terminus and involved three structural water molecules. This hydrogen bonding network is further influenced by Cys¹⁰⁵, Cys¹⁸⁰, Ser¹⁸¹, and Cys¹⁸². The assumed cysteine bond between Cys¹⁰⁵ and Cys¹⁸² is shown. This model was used as a guide to target residues for mutagenesis. Oxygens are colored red, nitrogens blue, carbons gray, and hydrogens green. A hydrogen bond interaction between atoms is specified with a dashed blue line. Where necessary, the blue line is bent for visual aesthetics only. (B) Predicted hydrogen bond network derived from homology modeling in the extracellular domain of the single-amino acid substitution mutants VCOP L280G (left) and L280P (right). Both mutant protein models indicate an interaction with Thr²⁸⁴ not present in WT VCOP. In the L280G model, the hydrogen bond interaction between the EC3 and EC2 loops is disturbed, whereas in L280P, the hydrogen bonds are shifted. Oxygens are colored red, nitrogens blue, carbons gray, and hydrogens green. A hydrogen bond interaction between atoms is specified with a dashed blue line. Where necessary, the blue line is bent for visual aesthetics only.

mutant. These results suggest there are specific interactions of Ser¹⁸¹ with other residues that do not tolerate even small changes, such as those found in Thr or Cys. Surprisingly, E176 and S181 single mutants had glycosylation patterns similar to that of WT VCOP and even some localization in the plasma membrane. These data suggest that the mutations to E176 and S181 induce a specific defect in the binding pocket rather than a global misfolding of the protein. In summary, Glu¹⁷⁶ and Ser¹⁸¹ in VCOP are both essential for proper protein folding and stabilization of the chromophore binding site.

A chimera model of the protein was produced by mutating the entire EC2 loop of VCOP to match residues from rhodopsin. No chromophore was detected in either the rhodopsin EC2 loop

chimera or the chimera Y186W mutant. These chimera mutants suggest that a stable retinal binding pocket requires very specific interacting residues in VCOP (Figure 6). The EC2 loop chimera models predict a disruption of the β -strands, yielding a more random coil-like structure for the EC2 residues. Differences in the intramolecular interactions between helices TM4 and TMS and a peptide consisting of the last five amino acids of the EC2 loop (¹⁸⁹VGTKYR¹⁹⁴ in WT VCOP and ¹⁹⁴PHEETN¹⁹⁹ in bovine rhodopsin) were also noted. The most significant difference is the H-bonding pattern along the β -strands. The WT VCOP model suggests that the backbone of Arg¹⁷², Met¹⁷⁴, and Glu¹⁷⁶ forms H-bonds with Asp¹⁸⁵, Gly¹⁸³, and Ser¹⁸¹, respectively, with an

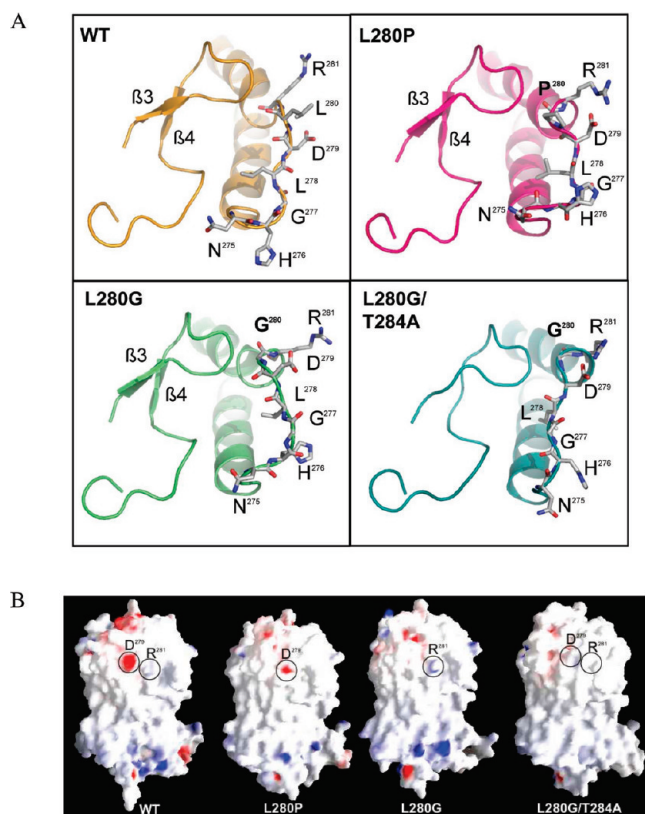


Figure 5. (A) Changes in conformation of the extracellular loop region accompany substitution of L^{280} . Ribbon representation of EC2 and EC3 with selected amino acid residues (portions of TM6 and TM7 are also shown in the background). The orientation of the EC3 residue side chains with respect to the EC2 loop is altered in all of the mutants. The WT VCOP protein displays a β -strand orientation similar to that of bovine rhodopsin, whereas the double mutant L280G/T284A shows significant disruption of the β -strand formation. These models suggest that partial misfolding of the EC region alters the ability of the mutants to stably bind 11-*cis*-retinal. (B) Charge density model of WT VCOP and EC3 VCOP mutants. The charge density of each residue is colored either red (negative) or blue (positive). The absence of charge is indicated by white. D^{279} and R^{281} are shown for each model. The charge density model indicates the L280G or -P mutation induces an interaction between D^{279} and R^{281} in which the charge on each moiety is partially or completely neutralized.

average distance between β -strands of 2.06 Å. Comparatively, the EC2 loop chimera model predicts no H-bond formation in the analogous residues, yielding a widening of up to 3.39 Å. PM6 semiempirical minimization of the protein generated data that reinforced the predictions of the CHARMM models. The distance between β -strands was predicted to increase by 2.5 Å, along with a 4.2° increase in the angle between the β -strands. The total root-mean-square shift of the center of mass of selected key residues predicted was 3.8 Å. These β -strand disruptions destabilize the EC2 loop interactions with the 11-*cis*-retinal in the chimera model and consequently prevent the Y186W mutant from binding retinal despite the increase in the level of favorable chromophore interaction with the mutant. In summary, computational models predict the manner in which Glu¹⁷⁶ and Ser¹⁸¹ stabilize the binding of the chromophore, as well as the sensitivity of the EC2 loop to mutation.

Conserved Residues in the EC2 Loop. Four conserved residues among the SWS1 pigments, Leu¹⁷⁸, Gly¹⁸³, Pro¹⁸⁴,

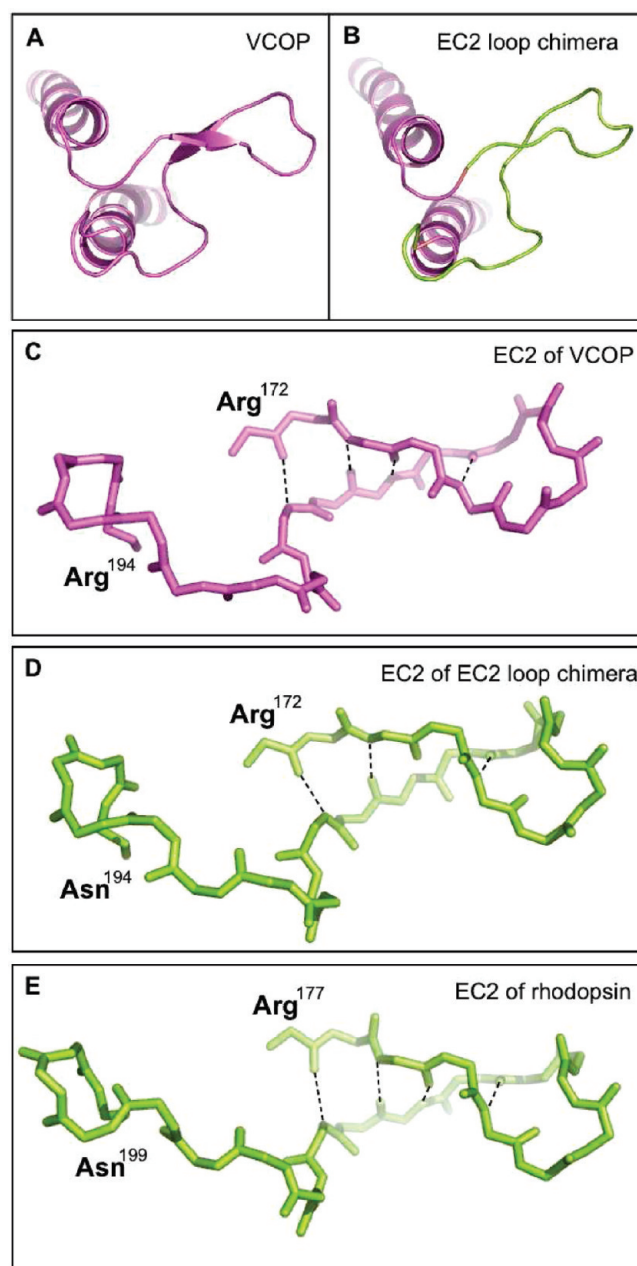


Figure 6. Ribbon diagram of EC2 loop chimera models. The WT VCOP model EC2 loop is shown in panel A, along with portions of TM2 and TM3. A model of the EC2 loop chimera VCOP protein is shown in panel B in the same orientation. The β -strands of the EC2 loop are shown for WT VCOP (C), the EC2 loop chimera (D), and bovine rhodopsin (E). As shown, fewer H-bonding interactions are observed in the chimera model than in either WT protein.

and Trp¹⁸⁶, in the EC2 loop have important functional properties. All four mutations of Leu¹⁷⁸ (to M, A, H, and D) weakened retinal binding significantly or completely and were predicted to be enthalpically disfavored. Leu¹⁷⁸ is predicted to coordinate the turn connecting the two EC2 β -strands. Shortening the $\beta 3$ strand by a E176G mutation together with a reintroduction of Glu at position 178 in the double mutant E176G/L178E did not lead to binding of the chromophore. PM6 minimization indicated the double mutant was enthalpically disfavored, and a 2° widening of the hairpin turn between β -strands was predicted. At position

178, the structural requirements for proper folding are truly only exhibited by Leu and Met and not by Ala, His, or Asp. The mutant models all predict disruptions of the two β -strands.

In addition to Leu¹⁷⁸, conserved residues Pro¹⁸⁴ and Gly¹⁸³ are shown to facilitate a turn so that the EC2 loop goes out of the binding crevice quickly. Substitution of Pro¹⁸⁴ with Ile led to weaker binding of retinal (50%) in the mutant protein and a slight change in λ_{max} (426 nm). Semiempirical minimization suggests the mutation is enthalpically unfavored and that the angle between strands β 3 and β 4 increases by 12°. The reduced level of retinal binding is due to the EC2 loop moving above the chromophore binding crevice, which reorients the two β -strands over 11-*cis*-retinal. This could either affect the interaction between the chromophore and protein or prevent or destabilize the formation of the putative disulfide bond between Cys¹⁰⁵ and Cys¹⁸².

The fourth conserved residue in the SWS1 pigments is a Trp at position 186 in VCOP. The indole ring of this residue, together with the phenolic ring of Tyr²⁶³, may have van der Waals interactions with the retinylidene polyene chain. The W186Y mutant had a barely detectable chromophore that likely could be the result of a weakened attractive interaction with the chromophore because the phenolic ring is significantly smaller than an indole ring. Although little structural change compared to WT was predicted in the PM6 minimization of the W186Y protein, the mutation is predicted to be enthalpically unfavored.

CONCLUSIONS

The importance of the extracellular (EC) loops in the proper folding of a short-wavelength sensitive 1 pigment has been elucidated via computational modeling, mutagenesis, and spectroscopic experiments. Despite the seemingly high flexibility in the EC loops as a whole, several EC loop residues have been identified as being critical for either the stabilization of the chromophore binding site or a more global folding, e.g., stabilization of the helical bundle. Specifically, four novel features of cone opsin proteins have been determined.

First, a H-bonding network that connects the EC2 loop, EC3 loop, and the N-terminus of the protein has been predicted via computational modeling. Although the EC3 loop of bovine rhodopsin is H-bonded to the N-terminus, there are no H-bonds connecting the EC2 and EC3 loops. The network in VCOP dictates the importance of the charged pair, Asp²⁷⁹ and Arg²⁸¹, which is conserved only among the SWS1 pigments. These residues function to stabilize the helical bundle and also orient a third conserved residue, Leu²⁸⁰, which facilitates the H-bonding between the EC2 and EC3 loops. Mutations to the SWS1 conserved ²⁷⁹DLR²⁸¹ motif have been shown to yield a misfolded protein.

Second, a disulfide bond between a residue in TM3, Cys¹⁰⁵, and a residue in EC2, Cys¹⁸², has been assigned on the basis of homology models with bovine rhodopsin. The nearby Cys¹⁸⁰ presents the possibility that the disulfide bond may be misassigned; however, mutagenesis experiments allow us to conclude that the correct assignment is a covalent linkage between Cys¹⁰⁵ and Cys¹⁸² via a disulfide bond. Furthermore, Western blotting and immunohistochemistry analysis indicate that the disulfide bond in VCOP is required for proper protein folding, whereas bovine rhodopsin tolerates substitution of the disulfide bond.¹⁸

Third, mutations of three residues in the β -strands of the EC2 loop (Leu¹⁷⁸, Pro¹⁸⁴, and Trp¹⁸⁶) conserved in cone pigments caused disruption of β -strand formation or formation of a hairpin turn. Proper hairpin formation was facilitated by either Leu or Met at position 178; however, improper formation resulted with

Ala, His, or Asp at position 178. Pro¹⁸⁴ directs the EC2 loop toward the binding site pocket. The weakened retinal binding observed for the P184I mutant due to a directional change in the EC2 loop results in the destabilization of favorable interactions of binding site residues with the chromophore, such as van der Waals attraction with the indole side chain of Trp¹⁸⁶. The direct correlation between a favorable van der Waals interaction of Trp¹⁸⁶ and the chromophore is shown by a decrease in the level of retinal binding in the W186Y mutant.

Fourth, mutations of two residues in the binding pocket of VCOP, Glu¹⁷⁶ and Ser¹⁸¹, have been explored and found to be important to the stability of chromophore binding. The analogous residues in bovine rhodopsin, Glu¹⁸¹ and Ser¹⁸⁶, can tolerate many substitutions with proper folding and small shifts in λ_{max} . However, in VCOP, the side chain length and charge on residue 176 must be conserved for proper folding. Small structural changes to the Ser residue at position 181, such as those found in S181C and S181T, also prevented binding of retinal. Western blotting and immunohistochemistry analysis indicate the mutations in VCOP induce a specific defect in the binding pocket rather than protein misfolding. Additional work is necessary to further characterize these findings.

AUTHOR INFORMATION

Corresponding Author

*B.E.K.: Department of Biochemistry and Molecular Biology, SUNY Upstate Medical University, 750 E. Adams St., Syracuse, NY 13210; telephone, (315) 464-8719; fax, (315) 464-8750; e-mail, knoxb@upstate.edu. R.R.B.: Department of Chemistry, University of Connecticut, Storrs, CT 06269; telephone, (860) 486-6720; fax, (860) 486-2981; e-mail, rbirge@uconn.edu.

Author Contributions

M.-H.C. and D.J.S. contributed equally to this work.

Funding Sources

This work was supported in part by National Institutes of Health Grants EY-11256 and EY-12975 (B.E.K.) and GM-34548 (R.R.B.), National Science Foundation Grants BES-0412387 and CCF-0432151 (R.R.B.), FONACIT Grant S1-2000000514 (J.B.), the Harold S. Schwenk Sr. Distinguished Chair funds for support of specialized instrumentation at the University of Connecticut, Research to Prevent Blindness (Unrestricted Grant to SUNY Upstate Medical University Department of Ophthalmology), and Lions of CNY.

ACKNOWLEDGMENT

We thank C. Kuemmel and M. Haeri for excellent technical assistance in optimizing Western blots and for valuable help with the immunohistochemistry of transfected cells.

ABBREVIATIONS

SWS1, short-wavelength sensitive 1 pigment; SWS2, short-wavelength sensitive 2 pigment; Rh1, rhodopsin; Rh2, rhodopsin-like pigment; LWS, long-wavelength sensitive pigment; VCOP, *Xenopus laevis* violet cone opsin; EC, extracellular; TM, transmembrane; CP, cytoplasmic.

REFERENCES

- (1) Okada, T., Sugihara, M., Bondar, A. N., Elstner, M., Entel, P., and Buss, V. (2004) The retinal conformation and its environment in

rhodopsin in light of a new 2.2 Å crystal structure. *J. Mol. Biol.* 342, 571–583.

(2) Palczewski, K., Kumasaka, T., Hori, T., Behnke, C. A., Motoshima, H., Fox, B. A., Le Trong, I., Teller, D. C., Okada, T., Stenkamp, R. E., Yamamoto, M., and Miyano, M. (2000) Crystal structure of rhodopsin: A G protein-coupled receptor. *Science* 289, 739–745.

(3) Teller, D. C., Okada, T., Behnke, C. A., Palczewski, K., and Stenkamp, R. E. (2001) Advances in determination of a high-resolution three-dimensional structure of rhodopsin, a model of G-protein-coupled receptors (GPCRs). *Biochemistry* 40, 7761–7772.

(4) Okada, T., Fujiyoshi, Y., Silow, M., Navarro, J., Landau, E. M., and Shichida, Y. (2002) Functional role of internal water molecules in rhodopsin revealed by X-ray crystallography. *Proc. Natl. Acad. Sci. U.S.A.* 99, 5982–5987.

(5) Altenbach, C., Cai, K., Klein-Seetharaman, J., Khorana, H. G., and Hubbell, W. L. (2001) Structure and function in rhodopsin: Mapping light-dependent changes in distance between residue 65 in helix TM1 and residues in the sequence 306–319 at the cytoplasmic end of helix TM7 and in helix H8. *Biochemistry* 40, 15483–15492.

(6) Klein-Seetharaman, J., Hwa, J., Cai, K., Altenbach, C., Hubbell, W. L., and Khorana, H. G. (2001) Probing the dark state tertiary structure in the cytoplasmic domain of rhodopsin: Proximities between amino acids deduced from spontaneous disulfide bond formation between Cys316 and engineered cysteines in cytoplasmic loop 1. *Biochemistry* 40, 12472–12478.

(7) Cai, K., Klein-Seetharaman, J., Hwa, J., Hubbell, W. L., and Khorana, H. G. (1999) Structure and function in rhodopsin: Effects of disulfide cross-links in the cytoplasmic face of rhodopsin on transducin activation and phosphorylation by rhodopsin kinase. *Biochemistry* 38, 12893–12898.

(8) Farrens, D. L., Altenbach, C., Yang, K., Hubbell, W. L., and Khorana, H. G. (1996) Requirement of rigid-body motion of transmembrane helices for light activation of rhodopsin. *Science* 274, 768–770.

(9) Resek, J. F., Farrahbakhsh, Z. T., Hubbell, W. L., and Khorana, H. G. (1993) Formation of the meta II photointermediate is accompanied by conformational changes in the cytoplasmic surface of rhodopsin. *Biochemistry* 32, 12025–12032.

(10) Klein-Seetharaman, J., Yanamala, N. V., Javeed, F., Reeves, P. J., Getmanova, E. V., Loewen, M. C., Schwalbe, H., and Khorana, H. G. (2004) Differential dynamics in the G protein-coupled receptor rhodopsin revealed by solution NMR. *Proc. Natl. Acad. Sci. U.S.A.* 101, 3409–3413.

(11) Tachibanaki, S., Arinobu, D., Shimauchi-Matsukawa, Y., Tsushima, S., and Kawamura, S. (2005) Highly effective phosphorylation by G protein-coupled receptor kinase 7 of light-activated visual pigment in cones. *Proc. Natl. Acad. Sci. U.S.A.* 102, 9329–9334.

(12) Terakita, A., Yamashita, T., Nimbari, N., Kojima, D., and Shichida, Y. (2002) Functional interaction between bovine rhodopsin and G protein transducin. *J. Biol. Chem.* 277, 40–46.

(13) Tachibanaki, S., Imai, H., Terakita, A., and Shichida, Y. (1998) Identification of a new intermediate state that binds but not activates transducin in the bleaching process of bovine rhodopsin. *FEBS Lett.* 425, 126–130.

(14) Phillips, W. J., and Cerione, R. A. (1994) A C-terminal peptide of bovine rhodopsin binds to the transducin α -subunit and facilitates its activation. *Biochem. J.* 299 (Part 2), 351–357.

(15) Shimauchi-Matsukawa, Y., Aman, Y., Tachibanaki, S., and Kawamura, S. (2005) Isolation and characterization of visual pigment kinase-related genes in carp retina: Polyphyly in GRK1 subtypes, GRK1A and 1B. *Mol. Vision* 11, 1220–1228.

(16) Raman, D., Osawa, S., and Weiss, E. R. (1999) Binding of Arrestin to Cytoplasmic Loops Mutants of Bovine Rhodopsin. *Biochemistry* 38, 5117–5123.

(17) Conner, M., Hawtin, S. R., Simms, J., Wootten, D., Lawson, Z., Conner, A. C., Parslow, R. A., and Wheatley, M. (2007) Systematic Analysis of the Entire Second Extracellular Loop of the V1A Vasopressin Receptor. *J. Biol. Chem.* 282, 17405–17412.

(18) Doi, T., Molday, R. S., and Khorana, H. G. (1990) Role of the intradiscal domain in rhodopsin assembly and function. *Proc. Natl. Acad. Sci. U.S.A.* 87, 4991–4995.

(19) Yan, E. C., Kazmi, M. A., De, S., Chang, B. S., Seibert, C., Marin, E. P., Mathies, R. A., and Sakmar, T. P. (2002) Function of extracellular loop 2 in rhodopsin: Glutamic acid 181 modulates stability and absorption wavelength of metarhodopsin II. *Biochemistry* 41, 3620–3627.

(20) Kaushal, S., and Khorana, H. G. (1994) Structure and function in rhodopsin. 7. Point mutations associated with autosomal dominant retinitis pigmentosa. *Biochemistry* 33, 6121–6128.

(21) Karnik, S. S., Sakmar, T. P., Chen, H. B., and Khorana, H. G. (1988) Cysteine residues 110 and 187 are essential for the formation of correct structure in bovine rhodopsin. *Proc. Natl. Acad. Sci. U.S.A.* 85, 8459–8463.

(22) Yan, E. C., Kazmi, M. A., Ganim, Z., Hou, J. M., Pan, D., Chang, B. S., Sakmar, T. P., and Mathies, R. A. (2003) Retinal counterion switch in the photoactivation of the G protein-coupled receptor rhodopsin. *Proc. Natl. Acad. Sci. U.S.A.* 100, 9262–9267.

(23) Davidson, F. F., Loewen, P. C., and Khorana, H. G. (1994) Structure and function in rhodopsin: Replacement by alanine of cysteine residues 110 and 187, components of a conserved disulfide bond in rhodopsin, affects the light-activated metarhodopsin II state. *Proc. Natl. Acad. Sci. U.S.A.* 91, 4029–4033.

(24) Anukanth, A., and Khorana, H. G. (1994) Structure and function in rhodopsin. Requirements of a specific structure for the intradiscal domain. *J. Biol. Chem.* 269, 19738–19744.

(25) Felline, A., Seeber, M., Rao, F., and Fanelli, F. (2009) Computational Screening of Rhodopsin Mutations Associated with Retinitis Pigmentosa. *J. Chem. Theory Comput.* 5, 2472–2485.

(26) Yuan, C., Kuwata, O., Liang, J., Misra, S., Balashov, S. P., and Ebrey, T. G. (1999) Chloride binding regulates the Schiff base pK in gecko P521 cone-type visual pigment. *Biochemistry* 38, 4649–4654.

(27) Ahuja, S., Hornak, V., Yan, E. C., Syrett, N., Goncalves, J. A., Hirshfeld, A., Ziliox, M., Sakmar, T. P., Sheves, M., Reeves, P. J., Smith, S. O., and Eilers, M. (2009) Helix movement is coupled to displacement of the second extracellular loop in rhodopsin activation. *Nature* 16, 168–176.

(28) Correa, S. A. A., Pignatari, G. C., Ferro, R. S., Pacheco, N. A. S., Costa-Neto, C. M., Pesquero, J. B., Oliveira, L., Paiva, A. C. M., and Shimuta, S. I. (2006) Role of the Cys18–Cys274 disulfide bond and of the third extracellular loop in the constitutive activation and internalization of angiotensin II type I receptor. *Regul. Pept.* 134, 132–140.

(29) Scarselli, M., Li, B., Kim, S. K., and Wess, J. (2007) Multiple Residues in the Second Extracellular Loop Are Critical for M3 Muscarinic Acetylcholine Receptor Activation. *J. Biol. Chem.* 282, 7385–7396.

(30) Kortagere, S., Roy, A., and Mehler, E. L. (2006) Ab initio computational modeling of long loops in G-protein coupled receptors. *J. Comput.-Aided Mol. Des.* 20, 427–436.

(31) Nikiforovich, G. V., Taylor, C. M., Marshall, G. R., and Baranski, T. J. (2010) Modeling the possible conformations of the extracellular loops in G-protein-coupled receptors. *Proteins* 78, 271–285.

(32) Nikiforovich, G. V., and Marshall, G. R. (2005) Modeling Flexible Loops in the Dark-Adapted and Activated States of Rhodopsin, a Prototypical G-Protein Coupled Receptor. *Biophys. J.* 89, 3780–3789.

(33) Nikiforovich, G. V., and Marshall, G. R. (2003) 3D model for Meta-II rhodopsin, An activated G-protein-coupled receptor. *Biochemistry* 42, 9110–9120.

(34) Vought, B. W., Dukkipati, A., Max, M., Knox, B. E., and Birge, R. R. (1999) Photochemistry of the primary event in short-wavelength visual opsins at low temperature. *Biochemistry* 38, 11287–11297.

(35) Kusnetzow, A., Dukkipati, A., Babu, K. R., Singh, D., Vought, B. W., Knox, B. E., and Birge, R. R. (2001) The photobleaching sequence of a short-wavelength visual pigment. *Biochemistry* 40, 7832–7844.

(36) Starace, D. M., and Knox, B. E. (1997) Activation of transducin by a *Xenopus* short wavelength visual pigment. *J. Biol. Chem.* 272, 1095–1100.

(37) Marti-Renom, M. A., Stuart, A. C., Fiser, A., Sanchez, R., Melo, F., and Sali, A. (2000) Comparative protein structure modeling of genes and genomes. *Annu. Rev. Biophys. Biomol. Struct.* 29, 291–325.

(38) Brooks, B., and Karplus, M. (1983) Harmonic dynamics of proteins: Normal modes and fluctuations in bovine pancreatic trypsin inhibitor. *Proc. Natl. Acad. Sci. U.S.A.* 80, 6571–6575.

- (39) Zhang, L., and Hermans, J. (1996) Hydrophilicity of cavities in proteins. *Proteins* 24, 433–438.
- (40) Kalé, L., Skeel, R., Bhandarkar, M., Brunner, R., Gursoy, A., Krawetz, N., Phillips, J., Shinozaki, A., Varadarajan, K., and Schulten, K. (1999) NAMD2: Greater scalability for parallel molecular dynamics. *J. Comput. Phys.* 151, 283–312.
- (41) Fong, S. L., Tsin, A. T., Bridges, C. D., and Liou, G. I. (1982) Detergents for extraction of visual pigments: Types, solubilization, and stability. *Methods Enzymol.* 81, 133–140.
- (42) Nicholls, A., Sharp, K. A., and Honig, B. (1991) Protein folding and association: Insights from the interfacial and thermodynamic properties of hydrocarbons. *Proteins* 11, 281–296.
- (43) Saam, J. (2010) Trajectory_smooth. http://www.ks.uiuc.edu/Research/vmd/script_library/scripts/trajectory_smooth/.
- (44) Russell, R. B., and Barton, G. J. (1992) Multiple protein sequence alignment from tertiary structure comparison: Assignment of global and residue confidence levels. *Proteins* 14, 309–323.
- (45) Babu, K. R., Dukupati, A., Birge, R. R., and Knox, B. E. (2001) Regulation of phototransduction in short-wavelength cone visual pigments via the retinylidene Schiff base counterion. *Biochemistry* 40, 13760–13766.
- (46) Stewart, J. J. P. (2008) MOPAC2009 Stewart Computational Chemistry, Colorado Springs, CO, [HTTP://OpenMOPAC.net](http://OpenMOPAC.net).
- (47) Guex, N., and Peitsch, M. C. (1997) SWISS-MODEL and the Swiss-PdbViewer: An environment for comparative protein modeling. *Electrophoresis* 18, 2714–2723.
- (48) Stewart, J. J. P. (2007) Optimization of Parameters for Semi-empirical Methods V: Modification of NDDO Approximations and Application to 70 Elements. *J. Mol. Model.* 13, 1173–1213.
- (49) G-Protein Couples Receptor Database version 8.1 (2004) <http://www.gpcr.org/7tm/>.
- (50) Molday, R. S., and MacKenzie, D. (1983) Monoclonal antibodies to rhodopsin: Characterization, cross-reactivity, and application as structural probes. *Biochemistry* 22, 653–660.
- (51) Li, J., Edwards, P. C., Burghammer, M., Villa, C., and Schertler, G. F. (2004) Structure of bovine rhodopsin in a trigonal crystal form. *J. Mol. Biol.* 343, 1409–1438.
- (52) Oprian, D. D., Molday, R. S., Kaufman, R. J., and Khorana, H. G. (1987) Expression of a synthetic bovine rhodopsin gene in monkey kidney cells. *Proc. Natl. Acad. Sci. U.S.A.* 84, 8874–8878.
- (53) Hwa, J., Klein-Seetharaman, J., and Khorana, H. G. (2001) Structure and function in rhodopsin: Mass spectrometric identification of the abnormal intradiscal disulfide bond in misfolded retinitis pigmentosa mutants. *Proc. Natl. Acad. Sci. U.S.A.* 98, 4872–4876.